JACS
JOURNAL OF THE AMERICAN CHEMICAL SOCIETY
Article
pubs.acs.org/JACS

Nanoporous Cobalt(II) MOF Exhibiting Four Magnetic Ground States and Changes in Gas Sorption upon Post-Synthetic Modification

Ming-Hua Zeng,*[,†] Zheng Yin,[†] Yan-Xi Tan,[†] Wei-Xiong Zhang,[‡] Yan-Ping He,[†] and Mohamedally Kurmoo[§]

[†]Department of Chemistry and Pharmaceutical Sciences, Guangxi Normal University, Key Laboratory for the Chemistry and Molecular Engineering of Medicinal Resources (Ministry of Education), Guilin, 541004, P. R. China

[‡]School of Chemistry and Chemical Engineering, Sun Yat-Sen University, Guangzhou, 510275, P. R. China

[§]Institut de Chimie de Strasbourg, CNRS-UMR 7177, Université de Strasbourg, 67070 Strasbourg Cedex, France

Supporting Information

ABSTRACT: We present the syntheses, structural characterization, gas sorption, I_2 uptake, and magnetic properties of a double-walled porous metal−organic framework, $[Co^{II}_3(lac)_2(pybz)_2]\cdot 3DMF$ (**1**·3DMF, purple, where pybz = 4-pyridyl benzoate, lac = D- and L-lactate) and of its post-synthetic modified (PSM) congeners, $[Co^{II}_3(lac)_2(pybz)_2]\cdot x$Guest ($x$Guest = 6MeOH, purple; 4.5EtOH, purple; 3PrOH, purple; $2C_6H_6$, purple; $2.7I_2$, black), $[Co^{II}_3(lac)_2(pybz)_2]$ (**1**, purple), $[Co^{II}_3(pybz)_2(lac)_2(H_2O)_2]\cdot 7H_2O$ (**1a**·$7H_2O$, green), and $[Co^{III}Co^{II}_2(pybz)_2(lac)_2(H_2O)_2]I\cdot 2H_2O\cdot 1.5$DMSO (**1b**·$I^-\cdot 2H_2O\cdot 1.5$DMSO, yellow, DMSO = dimethyl sulfoxide). Crystallography shows that the framework is not altered by the replacement of DMF by different solvents or by the removal of the solvent molecules during the single-crystal to single-crystal (SC-SC) transformations, while upon exchange with H_2O or partial oxidation by molecular iodine, the crystallinity is affected. **1** absorbs N_2, H_2, CH_4, CH_3OH, C_2H_5OH, PrOH, C_6H_6, and I_2, but once it is in contact with H_2O the absorption efficiency is drastically reduced. Upon PSM, the magnetism is transformed from a canted antiferromagnet (**1**·3DMF and **1**·xGuest) to single-chain magnet (**1**), to a ferrimagnet (**1a**·$7H_2O$), and to a ferromagnet (**1b**·$I^-\cdot 2H_2O\cdot 1.5$DMSO). Raman spectroscopy suggests the color change (purple to green **1a**·$7H_2O$ or yellow **1b**·$I^-\cdot 2H_2O\cdot 1.5$DMSO) is associated with a change of geometry from a strained octahedron due to the very acute chelating angle (~60°) of the lactate of a cobalt center to a regular octahedron with a monodentate carboxylate and one H_2O. The magnetic transformation is explained by the different interchain exchanges (J'), antiferromagnetic for **1**·3DMF and **1**·xSolvent ($J' < 0$), SCM for **1** (J' verge to 0), and ferromagnetic for **1a**·$7H_2O$ ($J' > 0$), between homometal topological ferrimagnetic chains (two octahedral and one tetrahedral Co^{II} ions) connected by the double walls of pybz at 13.3 Å (shortest Co···Co). For **1b**·$I^-\cdot 2H_2O\cdot 1.5$DMSO the moment of the tetrahedral site is turned off, thus stabilizing a ferromagnetic state ($J' > 0$). The present stabilization of four magnetic ground states is unique in the field of metal−organic frameworks as well as the electrical conductivity of **1**·$2.7I_2$.

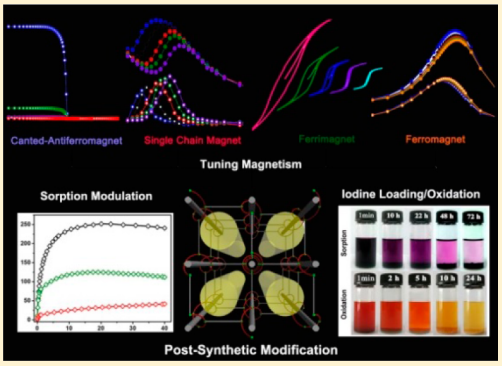

1. INTRODUCTION

Recently the multifunctionalization of microporous metal−organic frameworks (MMOFs) has become one of the principal focuses of inorganic and materials chemistry because multiple physical properties may coexist and even synergetically interact.[1] Therefore, better performance or tuning of functions or new applications is expected.[1,2] In this context, magnetic MMOFs especially those displaying long-range ordering are viewed as one of the significant candidates of multifunctional molecular materials.[3] In order to achieve long-range ordered magnetic materials one of the first requirement is the consideration of distance between the nearest-neighbors moment carriers.[4] In general, the critical temperature decreases exponentially with increasing the number of nonmagnetic atoms bridging the carriers. For example, metals have Curie temperature (T_C) approaching 1400 K, oxides have high T_C up to nearly 900 K, while for cyanides, the T_C is below 350 K, and those containing three-atom bridges are well below 50 K.[4] As such, one of us previously made the statement that long-range magnetic ordering and porosity are inimical based on the idea that long-range magnetic ordering requires a short connection between moment carriers and that porosity requires long ones.[5] This has been shown not to be the case under the condition that there are fragments containing M−O−M connections within the framework and weak magnetic interaction exists between them.[3,6] Thus, it is possible to classify the following four types of magnetic MMOFs: (i) organic molecules act as linkers between 1D inorganic M−O−M chains, so-called rod-spacer; (ii) organic pillars between inorganic M−O−M layers,

Received: January 8, 2014
Published: March 3, 2014

   dx.doi.org/10.1021/ja500191r | J. Am. Chem. Soc. 2014, 136, 4680−4688

so-called pillared-layer; (iii) organic molecules sitting in the gallery of inorganic M−O−M layers; and (iv) organic ligands connecting discrete M−O−M clusters, containing two or more metal ions or isolated metal ions, so-called cluster base MMOFs. The same analogy can be done for cyanides, but their transition temperatures for layer and chain compounds are expected to be lower than those with M−O−M connections.[3c]

Among the rod-spacer compounds of type I the magnetic ground states of $Co_3(OH)_2(C_4O_4)_2\cdot 3H_2O$[7] and $Ni_3(OH)_2(1,4\text{-chdc})_2(H_2O)_4\cdot 2H_2O$[8] were found to be modified by the presence of the lattice water. In the presence of water both are antiferromagnet, while in the absence the former is a ferromagnet and the latter is a ferrimagnet. Presumably the electron density of the solvent molecules introduces a weak antiferromagnetic exchange between the magnetic chains. Thus, the magnetic properties of these two compounds and also others established the importance of the solvents in magnetic MMOFs in contributing to the exchange.[9] Therefore, we may anticipate that if the chains are connected by longer nonmagnetic ligands and in the absence of solvent in the cavities, the chains may behave as single-chain magnets, while in the presence of solvent they may exhibit long-range ordering.[6,10] Using the same arguments, those of type IV would be single molecule magnet.[11] Many more examples showing modulation of T_C, T_N, or magnetic hysteresis have since been reported but only few show changes of ground state and usually two at most,[3,6−8,12] which was mainly due to the removal/inclusion/exchange of guest molecules (Table S1). In porous 3D framework, such transformation from an antiferromagnet to ferromagnet, ferrimagnet even single-chain magnet, single molecule magnet is rarely observed.[13] On the other hand, in rod-spacer MMOFs, the introduction of longer ligand is possible and beneficial for generating large voids. Hence, we expect magnetic MMOFs with rod-spacer feature to be a typical model to investigate magnetic switching behavior and also a good candidate of multifunctional molecular materials.

In order to test the above hypothesis, we made the cobalt analogue $[Co^{II}_3(lac)_2(pybz)_2]\cdot 3DMF$ (**1**·3DMF, purple) of the only double-walled framework, $[Zn_3(pybz)_2(lac)_2]\cdot 2.5DMF$, which has been shown to contain M−O−M connectivity within the well-separated square chains.[14] Solvent exchanged $[Co^{II}_3(lac)_2(pybz)_2]\cdot x$Solvent (*x*Solvent = 6MeOH, purple; 4.5EtOH, purple; 3PrOH, purple; $2C_6H_6$, purple), iodine loaded $[Co^{II}_3(lac)_2(pybz)_2]\cdot 2.7I_2$ (**1**·2.7I_2, black), and desolvated $[Co^{II}_3(lac)_2(pybz)_2]$ (**1**, purple) were obtained in SC-SC manner and the magnetic behaviors were investigated to reveal the relevance between host−guest interaction and magnetic ground state. Furthermore, given that post-synthetic modification (PSM) can modify either the organic linker or the coordination of the metal center without perturbing the parent framework and modify its physical properties,[15,16] we successfully conducted PSM on **1** by coordination and oxidation of the metal center to obtain two derivatives, hydrated $[Co^{II}_3(pybz)_2(lac)_2(H_2O)_2]\cdot 7H_2O$ (**1a**·7H_2O) and partially oxidized $[Co^{III}Co^{II}_2(pybz)_2(lac)_2(H_2O)_2]I\cdot 2H_2O\cdot$ 1.5DMSO (**1b**·I^-·2H_2O·1.5DMSO). Here, we report the syntheses, structures, interconversions, Raman spectra, thermal stability, gas sorption, and magnetic properties of these compounds (Scheme 1). As-prepared **1**·3DMF, solvent exchanged **1**·*x*Solvent, and I_2 loaded **1**·2.7I_2 behave as canted antiferromagnets, while upon desolvation **1** behaves as a single-chain magnet, and **1** is transformed into a ferrimagnet when it is

Scheme 1. Post-Synthetic Modifications and Resulting Magnetic Ground States and Changes in Coordination and Valence of Cobalt Ions

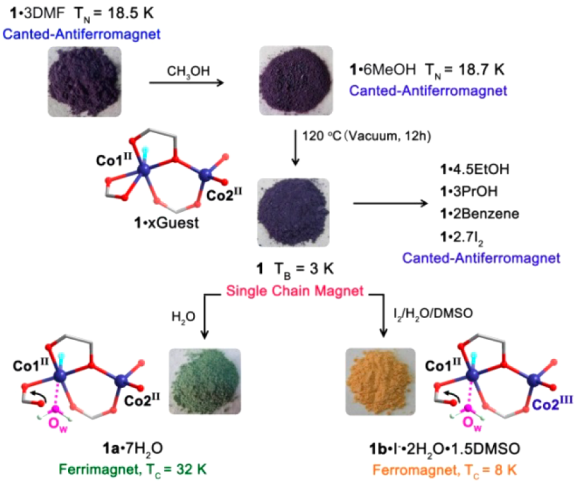

hydrated **1a**·7H_2O. By partial oxidation of **1** or **1a**·7H_2O by I_2 in DMSO/H_2O ferromagnetic **1b**·I^-·2H_2O·1.5DMSO is obtained. These changes were possible by the PSM of the as-prepared **1**·3DMF which alters the magnetic exchange interaction between the chains of cobalt ions from being antiferromagnetic through the electron density of the guests in the channel, to being nonexistent in the desolvated **1**, and finally to ferromagnetic through H_2O and DMSO. The series of compound realize for the first time the switching between four ground states by the modulation of host−guest interaction, magnetic M−O−M chain, and also the oxidation state of the spin carrier.

2. EXPERIMENTAL SECTION

2.1. Syntheses of the Compounds. *$[Co^{II}_3(pybz)_2(lac)_2]\cdot 3DMF$ (**1**·3DMF).* A DMF/1,2-propanediol (10 mL/6 mL) mixture containing $Co(NO_3)_2\cdot 6H_2O$ (350 mg, 1.2 mmol), 4-(pyridin-4-yl) benzoic acid (Hpybz) (199 mg, 1.0 mmol), and D-/L-H_2lac (90 mg, 1.0 mmol) in a Teflon-lined steel autoclave was heated at 110 °C for 3 days. After the autoclave has been cooled at a rate of 10 °C h^{-1} to 25 °C, the dark-purple ball-shaped crystals of **1**·3DMF were collected, washed with DMF, and dried in air (Yield: 65% based on Co). The phase purity of the bulk product was confirmed by powder X-ray diffraction (PXRD). Elemental analyses (%) calculated for **1**·3DMF: C, 48.36; H, 4.68; N, 7.23. Found: C, 48.29; H, 4.50; N, 7.11. IR (KBr, cm^{-1}): 3376(w), 2920(w), 2343(w), 1671(s), 1600(vs), 1558(vs), 1387(vs), 1120(w), 835(w), 775(m), 551(w), 481(w).

*$[Co^{II}_3(pybz)_2(lac)_2]\cdot x$Solvent (x*Solvent = 6MeOH; 4.5EtOH; 3PrOH; $2C_6H_6$).* Crystals of the **1**·6MeOH were obtained by soaking **1**·3DMF in dry methanol at room temperature for 3 days with renewal of the methanol several times. The crystals retain their purple color. Elemental analyses (%) calculated for **1**·6MeOH: C, 45.92; H, 5.13; N, 2.97. Found: C, 45.27; H, 4.63; N, 3.05. IR for **1**·6CH_3OH (KBr, cm^{-1}): 3360(b), 1566(vs), 1600(vs), 1392(vs), 1169(w), 1127(w), 1035(w), 1003(w), 827(w), 769(s), 688(w), 554(w), 472(w). While for **1**·4.5EtOH, **1**·3PrOH, and **1**·2C_6H_6, **1**·6MeOH were heated under dynamic vacuum at 100 °C for 2 h followed by soaking the desolvated crystals for 2 days in EtOH, PrOH, and C_6H_6, respectively. The content of different solvent molecules was calculated from the TG results.

*$[Co^{II}_3(lac)_2(pybz)_2]$ (**1**).* **1** was obtained by heating crystals of **1**·6CH_3OH under dynamic vacuum at 100 °C for 2 h. The crystals retain their purple color.

*$[Co^{II}_3(pybz)_2(lac)_2]\cdot 2.7I_2$ (**1**·2.7I_2).* Crystals of **1** (100 mg) were soaked in 20 mL 0.1 M cyclohexane solution of iodine for 8 days. The

dx.doi.org/10.1021/ja500191r | J. Am. Chem. Soc. 2014, 136, 4680−4688

black crystals were filtered and washed with 10 mL cyclohexane and dried in air. The maximum uptake is 0.9 g iodine per gram of **1**, corresponding to a formula of $[Co^{II}_3(lac)_2(pybz)_2]\cdot 2.7I_2$. Elemental analyses (%) calculated for $\mathbf{1}\cdot 2.7I_2$: C, 25.12; H, 1.69; N, 1.95. Found: C, 26.24; H, 1.83; N, 2.06.

*$[Co^{II}_3(pybz)_2(lac)_2(H_2O)_2]\cdot 7H_2O$ (**1a**·7H$_2$O).* **1a**·7H$_2$O was obtained by soaking crystals of **1** in water for 24 h. They turn to a jade green color. Elemental analyses (%) calculated for **1a**·7H$_2$O: C, 39.53; H, 4.64; N, 3.07. Found: C, 39.17; H, 4.83; N, 3.20. IR (KBr, cm^{-1}): 3136(bs), 1595(s), 1558(s), 1500(w), 1366(vs), 1076(w), 1035(w), 835(w), 777(s), 745(m), 562(w), 480(w).

*$[Co^{III}Co^{II}_2(pybz)_2(lac)_2(H_2O)_2]I\cdot 2H_2O\cdot 1.5DMSO$ (**1b**·I$^-$·2H$_2$O·1.5DMSO).* **1b**·I$^-$·2H$_2$O·1.5DMSO was obtained by soaking crystals of **1** in a solution of I$_2$ in DMSO/H$_2$O (v/v = 1:1) at 25 °C for 24 h and then washed with DMSO/H$_2$O (v/v = 1:1) and dried in air. The color of the crystals transform from dark purple to orange-yellow. Elemental analyses (%) calculated for **1b**·I$^-$·2H$_2$O·1.5DMSO: C, 37.20; H, 3.87; N, 2.63; S, 4.51. Found: C, 36.89; H, 3.73; N, 2.91; S, 4.42. IR (KBr, cm^{-1}): 3142(bs), 1600(s), 1552(s), 1514(m), 1371(s), 1183(w), 1035(w), 827(s), 772(s), 684(w).

2.2. General Methods. Thermogravimetric analyses (TGA) were performed on a Netzsch TG 209 instrument in flowing N$_2$ at a heating rate of 10 °C per minute in the range of 25 to 600 °C. PXRD measurements were performed on a Bruker D8 ADVANCE X-ray diffractometer with Cu-K$_\alpha$ radiation. PXRD measurements at different temperatures were recorded after the sample had been kept at the respective temperature for 20 min in flowing N$_2$. The crystalline powder samples were prepared by crushing the single crystals, and scans of 3−60° at a rate of 5°/min were recorded. Calculated PXRD patterns were generated using Mercury 3.0.[17] Raman spectra were obtained using a Renishaw inVia Raman microscope equipped with a 785 nm diode laser and a 1200 lines/mm grating. The N$_2$ sorption isotherm was recorded with an automatic volumetric adsorption apparatus (IGA-003 series, Hiden Isochema Ltd.) at 77 K. The benzene and methanol vapor sorption measurements were performed using a Belsorp-Max automatic volumetric adsorption apparatus. The high-pressure gas sorption measurements were performed using the Belsorp HP-60 high-pressure sorption system. Magnetizations of polycrystalline samples were measured in the temperature range of 2.0−300 K and field range ±50 kOe using a Quantum Design MPMS XL-5 SQUID magnetometer.

2.3. X-ray Diffraction. For the crystal structure determination, single crystals of **1**·3DMF, **1**·6CH$_3$OH, **1**·3PrOH, and **1**·2C$_6$H$_6$ were selected from batches covered with solvent and fixed to glass fiber for diffraction data collection at 173 K. However, for guest free **1**, the data were collected at 298 K using the crystal of **1**·6CH$_3$OH after the methanol was removed by heating the crystal at 355 K for 1 h on the diffractometer.

Single-crystal diffraction data were collected on a Bruker Smart Apex CCD diffractometer using graphite monochromated Mo-K$_\alpha$ radiation (λ = 0.71073 Å). Absorption corrections were applied by using multiscan program SADABS.[18] The structure was solved by direct methods and refined by full-matrix least-squares method on F^2 using the SHELXTL program package.[19] All nonhydrogen atoms except C15 were refined with anisotropic displacement parameters. The solvent molecules in **1**·3DMF and **1**·6CH$_3$OH were located from difference maps, and some of the solvent molecules were treated using a disorder model by dividing into parts with different occupancy ratio. Except for one C$_6$H$_6$ and one PrOH solvent molecule located from difference maps, other disordered guest molecules which cannot be modeled in **1**·2C$_6$H$_6$ and **1**·3PrOH were treated by the SQUEEZE routine,[20] and the amounts were determined by TGA results and elemental analyses. Hydrogen atoms of the organic ligands were refined using the riding model. Crystal data as well as details of data collections and refinements are summarized in Table S2. Selected bond distances and bond angles are listed in Table S3. The CCDC reference numbers are 978270−978274 for **1**·3DMF, **1**·6CH$_3$OH, **1**, **1**·3PrOH, and **1**·2C$_6$H$_6$, respectively. The supplementary crystallographic data for these compounds can be found in the Supporting Information or can be obtained free of charge from the Cambridge Crystallographic Data Centre via http://www.ccdc.cam.ac.uk/data_request/cif.

3. RESULTS AND DISCUSSION

3.1. Crystal Structures. The key feature of the five structures is the square pillars consisting of octahedral and tetrahedral cobalt ions and a racemic mixture of lactate ions (lac^{2-}) connected through the long pybz forming double walls between the pillars (Figure 1). The structure is the same as that

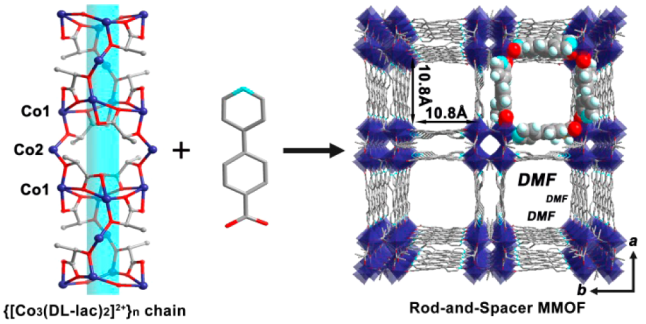

Figure 1. Schematic diagram of construction of a rod-spacer MMOF (H atoms are not shown for clarity). General color code: Co, indigo; N, turquoise; O, red; C, gray.

for the Zn analogue but **1**·3DMF crystallizes in the space group *P*-4c_2 instead of *P*-42$_1c$ for the Zn analogue. It contains two crystallographically distinct cobalt atoms in the ratio 2 (Co1, distorted octahedral):1 (Co2, tetrahedral) (Figure S1). Co1 is located on a general position and has a distorted octahedral geometry with five oxygen atoms [Co−O = 1.988−2.334 Å] of two lac and one pybz and one nitrogen atom [Co−N = 2.105 Å] of another pybz (Figure S2). Co2 is located at the 4*e* position and adopts a tetrahedral geometry with two deprotonated hydroxyl groups [Co−O = 1.905 Å] of two lac and two oxygen atom [Co−O = 1.963 Å] of carboxylate from two pybz. The lac exhibits η_5, μ_2, μ_2, μ_1-coordination modes, and the equivalent lac anions alternately link Co^{2+} into the square tubular $[Co_3(D\text{-}/L\text{-lac})_2]^{2+}$ chains parallel to the *c*-axis.

This chain can be viewed as a square with vertex of four equivalent six-coordinated Co^{2+} ions (Co1···Co1A distance of 4.391 Å) bridged by a single oxygen atom of a lac (Co1−O4−Co1 of 162.9°) linked by two four-coordinated Co^{2+} ions (Co1···Co2 distance of 3.424 Å) by two bridges of one oxygen atom and a *syn*−*syn* carboxylate of pybz (Co1−O3−Co2 of 123.1°) (Table 1, Table S4). The Co1−O4−Co1 angles for **1**·3DMF, **1**·6CH$_3$OH, **1**, **1**·2C$_6$H$_6$, and **1**·3PrOH are 163.0°,

Table 1. Selected Bond Distances and Bond Angles of Importance to Magnetic Exchanges Between Co(II) Ions[a]

	1·3DMF	**1**·6CH$_3$OH	**1**	**1**·3PrOH	**1**·2C$_6$H$_6$
Co1−O4[a]	2.334	2.327	2.424	2.336	2.311
O5[a]−Co1−O4[a]	59.5	59.4	57.9	58.7	59.7
Co1···Co2	3.424	3.421	3.426	3.414	3.434
Co1−O3−Co2	123.1	122.6	122.6	122.4	123.6
Co1···Co1[b]	4.391	4.385	4.467	4.397	4.369
Co1−O4−Co1[b]	163.0	162.6	164.3	162.8	162.5

[a]Symmetry codes: For **1**·3DMF, **1**·6CH$_3$OH and **1**·3PrOH, (a) $-y-1, x-1, -z$; (b) $y+1, -x-1, -z$. For **1**: (a) $-y+2, x, -z$; (b) $y, -x+2, -z$. For **1**·2C$_6$H$_6$: (a) $-y+1, x, -z$; (b) $y, -x+1, -z$.

dx.doi.org/10.1021/ja500191r | J. Am. Chem. Soc. 2014, 136, 4680−4688

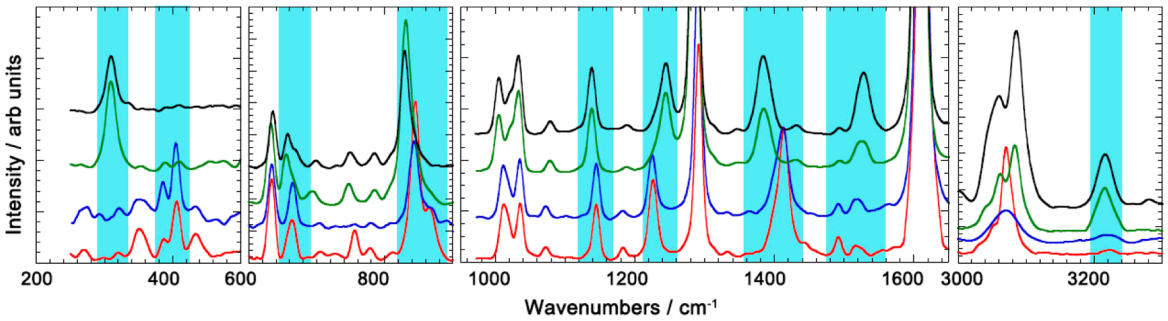

Figure 2. Raman spectra for **1**·3DMF (red), **1** (blue), **1a**·7H_2O (green), and **1b**·I^-·2H_2O·1.5DMSO (black), in which the sensitive peaks are highlighted.

162.6°, 164.3°, 162.5°, and 162.8°, respectively. It should be noted that the structure differs from previous linear, zigzag, ladder, helical, and ribbon chains widely found in 1D, 2D, or 3D coordination polymers which use a single metal center as node.[3d] The present thick and rigid chain can be viewed as constructed by their two square alternately connected vertexes (Figure 1). Such a feature renders both the chain and the framework high stability that is crucial for subsequent PSM.[15] Especially, the dominant M−O−M connectivity in the chain is crucial for magnetism, hence variation of such connectivity may greatly affect the magnetic behavior of the compound.[6]

These chains of cobalt are further linked by double pybz bridges along the *a* and *b* directions, forming a 3D neutral framework with square 1D channels which are occupied by guest solvent in **1**·*x*Solvent and empty in **1**. Taking the van der Waals radii of the atoms into consideration, using PLATON the window of these channels was estimated to be ca. 10.8 × 10.8 $Å^2$ (distance of pairs of the ligand constituted the opposite walls) with a solvent accessible volume of 43.1% of the unit cell.[20] The framework is retained for all five of the compounds except for the small variation of bond distances and angles. The very low residual electron density in the crystal structure analyses of **1** indicates that all of the CH_3OH has been removed from the channels. No global change in connectivity occurs in the framework upon desolvation except for minimal changes in metal−ligand bond distances and angles. The average coordination bond lengths of Co1 and Co2 in **1** are 2.120 and 1.943 Å, respectively, which are slightly longer than those [2.111 and 1.934 Å] of **1**·3DMF. This difference may be due to the higher temperature at which the data of **1** was collected. The solvents, 3DMF, 4.5EtOH, 6CH_3OH, 3PrOH, and 2C_6H_6 per molecular unit within the channels, are reasonable and quite compact even though most of them were refined in disorder models.

3.2. Thermal Properties. Thermogravimetric analyses of all the compounds show the destruction of the framework at ca. 400 °C. Before being destroyed it is stable for a wide temperature range over 200 °C (Figure S3, Table S5). Such thermal stability is comparable to the highly thermo-stable MMOFs[21] and can be associated with the strong intra- and inter-rod connection that also contributes to subsequent PSM. The solvents are removed slowly from room temperature in all cases, but the temperature at which all the solvents are removed differs from compound to compound. This temperature is an indication of the strength of the interaction between the solvent molecules and the solvent with the framework, and it increases in the order methanol < ethanol < propanol < benzene < DMF. Except for the anomalous temperature for benzene, the order respects the boiling point of the liquids, which suggests the solvent−solvent interaction cannot be ignored.

When the crystals of **1** are immersed in water or exposed to water vapor, they turn green. TGA of the green crystals **1a**·7H_2O exhibits gradual loss of water from room temperature with a step at ca. 165 °C (13.3%) and finishes at 250 °C (3.9%) (Figure S4). The first loss amounts to 7H_2O (calculated 13.8%) and the second to 2H_2O (calculated 4.0%) (Table S5). We infer that 7H_2O resides in the channels, and the other two are coordinated to the cobalt. The coordinated water to the highly distorted octahedral cobalt Co1 will force it to become more regular, and the color of that center is expected to be pink. Consequently, in the presence of the blue tetrahedral cobalt the overall color of the compound will appear green.[22]

3.3. Powder X-ray Diffraction. PXRD has been used to check the purity of the samples and also to study the structural changes that take place during certain modification. First the experimental PXRD of **1**·3DMF is the same as that calculated using the single crystal result (Figure S4). After desolvating, the PXRD of **1** is again similar to that calculated using the single crystal result. The temperature dependence of the transformation of **1**·3DMF to **1** was studied in situ, and it is found to be a smooth one with retention of the crystallinity. However, when **1** is soaked in water or exposed to water vapor it is transformed to a poorly crystalline material **1a**·7H_2O (Figure S5). The crystallinity is further deteriorated upon dehydrating of **1a**·7H_2O to [Co^{II}_3(pybz)$_2$(lac)$_2$] (**1′**). The XRD pattern for the latter appears to be very different to the original **1**. From the patterns no structural characteristics can be elucidated.

3.4. Raman and IR Spectroscopy. The Raman spectra (Figure 2) of **1**·3DMF, **1**, **1a**·7H_2O, and **1b**·I^-·2H_2O·1.5DMSO belong to two different classes, that is those without water in the crystals (**1**·3DMF and **1**) and those with (**1a**·7H_2O and **1b**·I^-·2H_2O·1.5DMSO). The bond energies and the differences between them for the two classes can be used to derive the coordination geometries of the metals and the modes of bonding of the ligands.[23] The Raman bands, which are not perturbed by the presence of water, are assigned to the organic ligand pybz. In contrast, the bands which are perturbed are assigned to the lactate ions and the metal−ligand vibrations. Our assumption, based on our previous work[24] and the crystallographic data reported by Bourne et al.,[25] is that the long bond and the strained coordination of the carboxylate of the lactate to Co1 are easily removed by the coordination of incoming water to give a regular octahedral Co1. The ν(OH) band of water for **1a**·7H_2O and **1b**·I^-·2H_2O·1.5DMSO is at 3216 cm^{-1}. The region of the carboxylate vibrations (1100−1450 cm^{-1}) has four intense bands which can be identified by

dx.doi.org/10.1021/ja500191r | J. Am. Chem. Soc. 2014, 136, 4680−4688

the difference between carboxylate ν_s(OCO) and ν_{as}(OCO).[23] The difference of ca. 146 cm^{-1} in the four compounds is consistent with that of a relaxed carboxylate, and thus we assigned these pairs of bands to the benzoate of pybz. In contrast for the highly strained lactate the difference is 188 cm^{-1} for **1**·3DMF and **1**, while it is reduced to 136 cm^{-1} upon solvation with water. Thus it is reasonable to assume that the long Co−O(lac) bond is broken while relieving the strain of the coordination.[24,25] This is associated to the color change from purple to green consistent with the change of electronic structure resulting in a lower extinction coefficient for the less distorted octahedral cobalt, which in the presence of the expected blue color of the tetrahedral cobalt will give a jade green color.[22] The bending modes lowering from 844 (**1**·3DMF and **1**) to 830 cm^{-1} (**1a**·7H_2O and **1b**·I^-·2H_2O·1.5DMSO) are again in line with the arguments presented above. For **1**·3DMF and **1**, the Co−O stretching modes are numerous in the range 350−450 cm^{-1}, which is due to the highly irregular octahedron around Co1 and they collapse into one band at 308 cm^{-1} for **1a**·7H_2O and **1b**·I^-·2H_2O·1.5DMSO.[24,25] As a comparison, the IR spectra of these four compounds were dominated by carboxyl groups and water guest molecules and also can be divided to two different classes like the Raman spectra. And the similar information further confirmed the structure transformations and the stability of the host framework (Figure S6). In the absence of crystal structures for **1a**·7H_2O and **1b**·I^-·2H_2O·1.5DMSO, the Raman and IR spectra were useful in elucidating the molecular structures and thus allow further discussion of structure−magnetic properties relationship.

3.5. Gas Sorption. The observation of a stable porous framework with large channels of 10.8 × 10.8 $Å^2$ after removal of the solvents prompted us to study the gas sorption properties especially in view of the presence of a surface having different potential sites for sorption. We have therefore study the sorption of gases (N_2, CO_2 up to 1 bar and H_2, CH_4 up to 40 bar) and solvent vapors (C_6H_6 and CH_3OH up to 1 bar) for **1** and **1′** (desolvated **1a**·7H_2O), respectively.

The N_2 sorption isotherm for **1** at 77 K shows a typical type I behavior with maximum uptake of 256 cm^3 g^{-1} (STP) at 1 bar (Figures 3 and S7), corresponding to a Langmuir surface area of 1050 m^2 g^{-1}, which is comparable to the Zn analog and among one of the highest for magnetic MMOFs (Table S6).[14,26] It demonstrates once again that the rod-spacer strategy is an effective method to construct magnetic MMOFs with large voids by the introduction of longer linker. In addition, **1** shows maximum H_2 and CH_4 uptake of 252 cm^3 g^{-1} (77 K, 40 bar) and 84.8 cm^3 g^{-1} (298 K, 39 bar), respectively (Figures 3 and S8). In contrast, **1′** has nearly no N_2 sorption. For high-pressure H_2 or CH_4 sorption, a similar phenomenon was also observed with a maximum uptake of 42 cm^3 g^{-1} (one-sixth of that of H_2 for **1**) and 11.4 cm^3 g^{-1} (one-eighth of that of CH_4 for **1**). Such results suggest that the 1D porous channel and/or the windows may shrink due to twist of the pybz linker during the transformation from **1** to **1a**·7H_2O driven by the change of the coordination of one of the cobalt ions.[24,27]

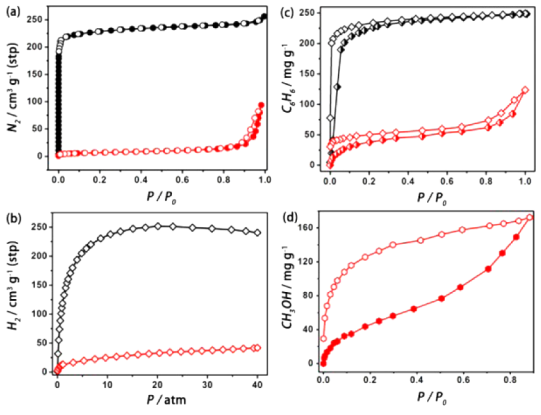

Figure 3. The sorption isotherms for **1** (black) and **1′** (red): (a) N_2 at 77 K; (b) H_2 at 77 K; (c) C_6H_6 at 298 K; (d) CH_3OH at 298 K.

For solvent vapor, **1** shows typical type I benzene sorption curve with saturated uptake of 249 mg g^{-1} (2.3 benzene molecule per formula unit) (Figure 3). Though sharing analogous sorption isotherm, the saturated benzene uptake of desolvated **1′** (124 mg g^{-1}, about 1.2 benzene molecule per formula unit) is just one-half of the value of **1**. Comparing to benzene, the sorption of MeOH increases slowly with the increase of vapor pressure and the maximum uptake was 172 mg g^{-1} (4.3 methanol molecule per formula unit) at P/P_0 = 0.88. This not fully saturated value compared to the methanol exchanged crystals **1**·6CH_3OH. Hence, methanol shows recovery ability of the shrinking channels of **1′**.

3.6. Enrichment versus Oxidation of 1 by I_2. In contrast to iodine uptake by the Zn analogue, the cobalt compound can uptake iodine as well as get oxidized. When crystals of **1** (100 mg) were soaked in aprotic cyclohexane solution of I_2 (3 mL of 0.1 M), the dark-violet coloration of the I_2 solution slowly fades to transparent light purple, and the resulting crystals become very dark purple to black (Figure 4).

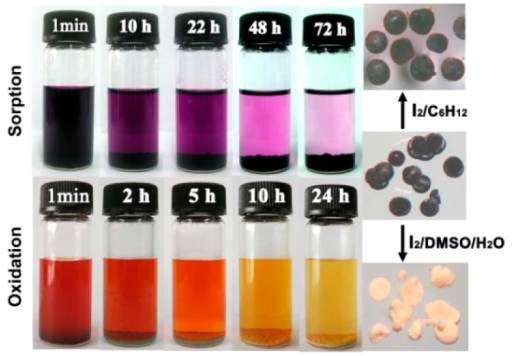

Figure 4. Photos of iodine sorption in cyclohexane (top) and iodine oxidation in DMSO/H_2O (1:1) (bottom). The purple crystals of **1** transform to black after sorption of iodine and to orange after being oxidized.

The uptake is 0.9 g iodine per gram of **1** to give [Co^{II}_3(lac)$_2$(pybz)$_2$]·2.7I_2 (**1**·2.7I_2, iodine content of 47.8%) which is close to that of the Zn analogue ([Zn_3(lac)$_2$(pybz)$_2$]·3I_2 (iodine content of 49.8%). The loading process appears to be slower for **1** (Figures S9 and S10).[14] The reverse process, that is I_2 release was monitored by UV−vis transmission spectroscopy by soaking some crystals of **1**·2.7I_2 in ethanol (Figure S11). The iodine absorption bands were found to increase slowly with time and tend toward saturation after 3 h. Two-probe electrical conductivity measurement on a powder sample, contacted with gold paint, shows an ohmic behavior in the voltage of −1 to 1 V (Figure S12). The conductivity (σ) is 7 × 10^{-6} S/cm for **1**·2.7I_2 which is higher than the 10^{-6} to 10^{-8} S/m found for the iodine-loaded single crystal of tris(*o*-

dx.doi.org/10.1021/ja500191r | J. Am. Chem. Soc. 2014, 136, 4680−4688

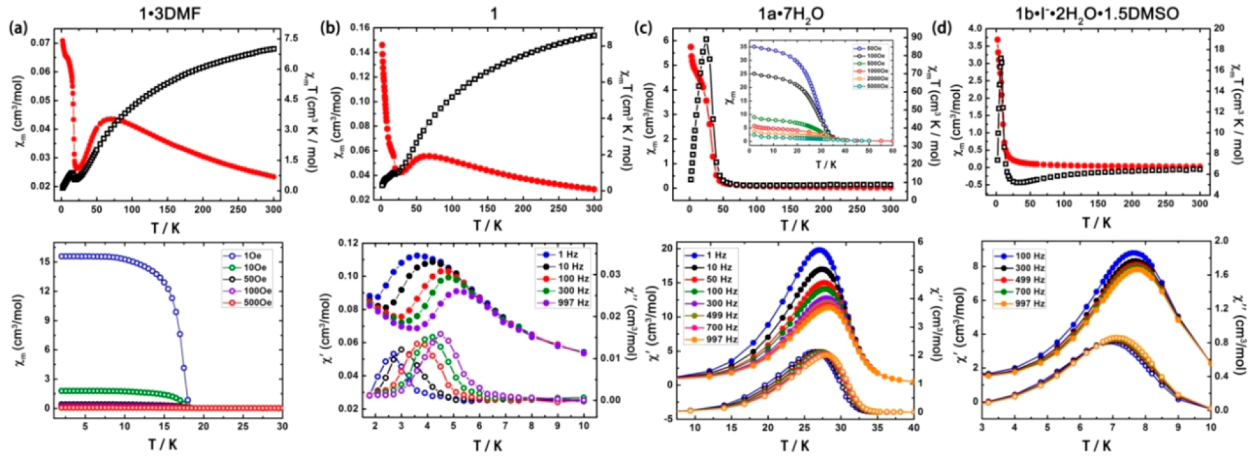

Figure 5. The temperature dependence of the dc and ac magnetic susceptibilities of four different magnetic ground states for (a) **1**·3DMF, (b) **1**, (c) **1a**·$7H_2O$, and (d) **1b**·I^-·$2H_2O$·1.5DMSO.

Table 2. Parameters Characterizing the Magnetic Properties of the Compounds

compounds	Curie constant C (cm^3 K/mol)[a]	Weiss constant Θ (K)[a]	critical temperature (K)[b]	canting angle (°)	M ($N\mu_B$)[c]
1·3DMF	10.25(4)	−137(1)	T_N = 18.5	0.05	0.34
1·$6CH_3OH$	9.54(4)	−94(2)	T_N = 18.7	0.08	1.47
1·4.5EtOH	10.48(3)	−137(2)	T_N = 17.5	0.21	0.20
1·3PrOH	9.52(8)	−115(3)	–	–	0.32
1·$2C_6H_6$	9.08(12)	−119(5)	–	–	0.42
1·$2.7I_2$	11.97(3)	−102(1)	T_N = 8	0.01	0.91
1	12.34(3)	−130(1)	T_B = 3	–	0.50
1a·$7H_2O$	9.08(11)	−13(3)	T_C = 32	–	5.23
1b·I^-·$2H_2O$·1.5DMSO	6.91(3)	−6(1)	T_C = 8	–	4.75

[a]Curie−Weiss fit of data between 150 and 300 K. [b]T_N, T_C, and T_B is Néel, Curie, and blocking temperature, respectively. [c]Magnetization at 2 K in 50 kOe.

phenylenedioxy) cyclotriphosphazene[28] but much less than that of the single crystal of the iodine-loaded Zn analogue of 3×10^{-3} ($\sigma_{\parallel}$) and 1×10^{-4} ($\sigma_{\perp}$) S/cm.[14]

However, when crystals of **1** were soaked in a DMSO/H_2O (v/v = 1:1) solution of iodine, the crystals slowly change color from purple to orange **1b**·I^-·$2H_2O$·1.5DMSO (Figure 4). Its PXRD shows very few peaks, which is common to that found for **1a**·$7H_2O$ and indicates that the two compounds are next to being amorphous (Figure S5). TGA shows two weight losses before the framework is destroyed at ca. 400 °C; the first at ca. 150 °C amounts to 15.6% which corresponds to $2H_2O$ and 1.5DMSO solvent molecules (Figure S3, Table S5). The elemental analysis results also coincide well with such a composition. The Raman spectrum shows a close similarity in band energies as that of **1a**·$7H_2O$ (Figure 2). Using similar arguments as above, we can assume that the lactate is now monodentate and that one water molecule is coordinated to each Co1. Since **1b**·I^-·$2H_2O$·1.5DMSO is not green but orange is a strong indication that the tetrahedral Co2 is no longer four coordinated but five or six. Thus, we propose that it is the Co2 that is oxidized favorably.[29] Therefore, only the Co1 will be moment carriers, and a reduction in moment is found as expected (see below).

3.7. Magnetic Properties. The magnetic properties of the compounds have been studied as a function of temperature, field, and ac frequencies (Figure 5). The results can be presented by the behavior at high and low temperatures. In high-temperature regions all the compounds behave as Curie−Weiss paramagnets with differing exchange interactions. Analyses of the high temperature data (150−300 K) have been performed in each case using the Curie−Weiss function (Table 2). From the analyses we find two classes: those (**1**·*x*Solvent, **1**·$2.7I_2$ and **1**) (Figures S13−18) with a fairly high Weiss temperature of ca. −130 K and those (**1a**·$7H_2O$ and **1b**·I^-·$2H_2O$·1.5DMSO) with ca. −10 K. The former compounds exhibit a broad maximum in the susceptibility at ca. 65 K and a minimum around 25 K. The temperature dependence between 25 and 300 K may be associated with low-dimensional behavior.

Considering the structural parameters, interatomic distances and angles (Table 1), we can define two principal exchange interactions within each chain where both are mediated through one single oxygen atom, that is J_1 (Co1−Co1) with Co···Co distance of 4.37−4.47 Å and Co1−O−Co1 angle of 162.5−164.3 and J_2 (Co1−Co2) with Co···Co of 3.41−3.43 Å and Co1−O−Co2 of 122.4−123.6.[21,30] From the interatomic distances we can intuitively assume that $|J_1| < |J_2|$. Secondary exchange interactions (J_3) exist for example Co1−Co2 at distances of about 6.09 Å and Co1−Co1 at 6.07 Å. The latter will be weak in comparison to the former ones. Between chains we can consider two interactions: J_4 through the connecting pybz bridge and dipolar through space and the other (J') through the solvents in the channels. The lack of magnetic ordering in **1** would suggest that J_4 is negligible.

In the case of **1**·*x*Solvent and **1**, the susceptibility in the high-temperature region can be interpreted as dominated by the strong antiferromagnetic coupling $J2$. As kT approaches ≈65 K the Co1−Co1 antiferromagnetic coupling, J_1, becomes

dx.doi.org/10.1021/ja500191r | J. Am. Chem. Soc. 2014, 136, 4680−4688

operative and further decrease the susceptibility. For **1**·*x*Solvent, the presence of solvents provides enough electron density to generate the weak interchain (J') interaction (Figure 6), and long-range magnetic ordering is observed at the same

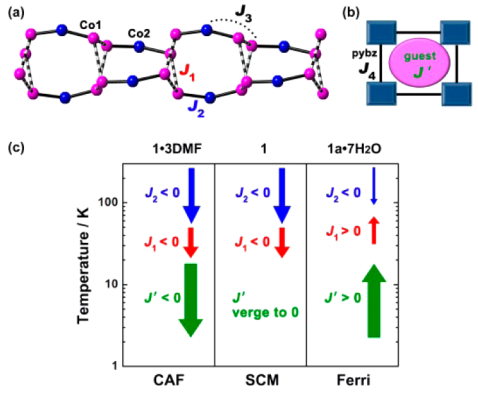

Figure 6. Representation of the (a) intrachain exchange interactions of J_1, J_2, and J_3 and (b) interchain exchange interactions of J_4 and J'. (c) The operative temperature region of relatively strong interaction of J_1, J_2, and J' to model the magnetic ground states.

temperature of 18 ± 1 K. The strong field dependence and the weak isothermal magnetization at 2 K indicate the ground state for these compounds is canted antiferromagnetic.[30] This is further confirmed by the low magnetization in high field. Using the magnetization (16 cm^3 G/mol) at 2 K measured in 1 Oe field cooling for **1**·3DMF and an expected saturation magnetization for a ferromagnetic chain of 3 μ_B (3 × 5585 cm^3 G/mol), the canting angle is estimated as 0.006°. For **1**·2.7I_2 the high-temperature behavior is almost the same, but the canting appears at lower temperature of 10 K (Figure S18) and ac susceptibilities independent of frequency of the ac field.

The high-temperature susceptibility behavior of **1** is similar to those of **1**·*x*Solvent (Figure 5), which indicate the interactions involved are of the same signs and magnitudes. However, the low-temperature behavior is quite different. There is no long-range order, and the magnetization increases continuously to the lowest temperature of 2 K. The ac susceptibilities of **1** in a 5 Oe field oscillating at different frequencies and a zero dc field exhibit strong frequency dependence. Both the in-phase (χ') and out-of-phase (χ'') susceptibilities peak temperatures shift with increasing frequency, for example, T_{max} (χ' shifts from 2.7 K at 1 Hz to 4.5 K at 997 Hz). The relaxation process is defined by the parameter $\phi = (\Delta T_{max}/T)/\Delta(\log \upsilon) = 0.12$, which is in agreement with that expected for superparamagnetism. The strong frequency-dependent behavior can be further confirmed by the Cole−Cole diagram at 3.5 K (Figure S19), which follows a generalized Debye model with $\alpha = 0.4$ ($R = 2.09 \times 10^{-5}$), indicating a relative narrow distribution of relaxation times. The relaxation time (τ) of **1** follows the Arrhenius behavior ($\tau = \tau_0 \exp(\Delta_\tau/k_BT)$), with $\Delta_\tau = 41(8)$ K and $\tau_0 = 1.7 \times 10^{-8}$ s ($R = 0.999$). Therefore, with these parameters we can imagine the chains are magnetically isolated and can be considered as single-chain magnets within a 3D framework.[31,32]

The high-temperature behavior of the susceptibility of **1a**•7H_2O belongs to the second class mentioned above. It does not show the broad maximum at 65 K and instead the susceptibility increases on cooling below 120 K (Figure 5). This indicates that J_1 is now ferromagnetic (Figure 6). To discuss the magnetic properties we have to recall that the Raman spectroscopy has indicated a change of geometry of Co1 from a highly distorted to a regular octahedron. Thus, this structural change has major effect on the susceptibility due to the change of the electronic structure and especially with the additional anisotropy of the Co1 in the regular octahedral geometry. The low Weiss temperature suggests the modification of the geometry of Co1 induces either a reduction in both J_1 and J_2.

The χ_mT versus T plot is characteristic of that of a ferrimagnet with a minimum at 100 K. The ZFC-FC magnetization in a field of 10 Oe exhibits a bifurcation temperature of 32 K (Figure S20). Both component of the ac susceptibilities are nonzero, and χ' has a peak at 27.0 K at 1 Hz which is shifted to 28.5 K at 1 kHz. χ'' becomes nonzero below 33 K, confirming a critical temperature of 32 ± 1 K, but the frequency dependence is weaker. The magnetization below 33 K is field dependent due to the long-range ordering. The isothermal magnetization at 2 K is hysteretic with a coercive field of 2.4 kOe, saturation magnetization at 50 kOe of 5.2 μ_B, and a remanant magnetization of 0.84 μ_B (Figures 7 and S20).

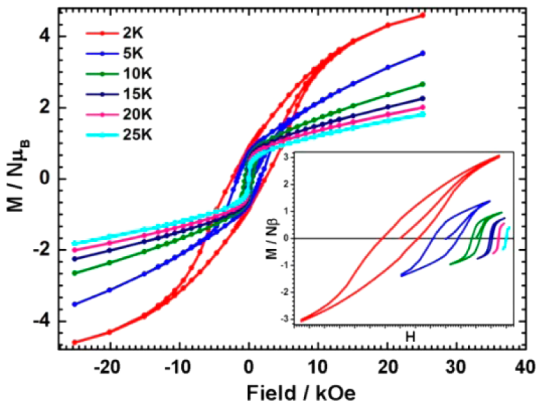

Figure 7. Isothermal magnetization at different temperatures for **1a**•7H_2O. Coercive field: 2400 Oe (2 K), 1650 Oe (5 K), 540 Oe (10 K), 150 Oe (15 K), 40 Oe (20 K), 10 Oe (25 K).

Both the coercive field and the remanant magnetization decrease upon warming. All the characteristics, except for the saturation magnetization of 5.2 μ_B, tend to the conclusion of a ferrimagnetic ground state.[33]

If the exchange interactions, J_1 and J_2, are antiferromagnetic we can have a situation as depicted in Figure 7, where the moments of two Co1 are antiparallel to the other two Co1 and to the two Co2. Assuming the moments of each chain are oriented equally in the same direction, then a ferrimagnet results but the saturation moment is expected to be 3 μ_B (that is +1 × 2.4 μ_B per Co1, −1 × 2.4 μ_B per Co1, +1 × 3 μ_B per Co2). To account for a saturation of 5.2 μ_B, we may invoke alignment of the moments of Co1 and Co2 along different axes given the different anisotropies. Thus, we propose one possible solution where the four Co1 moments, behaving as *xy*, point away from the center of the square in the *ab*-plane but with a canting along the *c*-axis and the Co2 moments, behaving as Ising, lie along the *c*-axis. The surplus moment requires that each Co1 moment be canted by $\sin^{-1}(1.1/2) = 3.66°$ from the *ab*-plane. Such a model requires neutron diffraction to confirm its validity, but such an experiment is not feasible due to the amorphous nature of the compound.

dx.doi.org/10.1021/ja500191r | J. Am. Chem. Soc. 2014, 136, 4680−4688

For **1b**·I^-·$2H_2O$·1.5DMSO, $\chi_m T$ is only 6.48 cm^3 mol^{-1} K at 300 K (Figure 5). On lowering temperature it is decreased to 5.22 cm^3 mol^{-1} K at 30 K before reaching a maximum of 16.11 cm^3 mol^{-1} K at 7.0 K. The Curie−Weiss fit of the high-temperature data gives a negative θ of −6(1) K and C = 6.91 cm^3 mol^{-1} K. Both the ac susceptibilities show a peak at ca. 7 K which is independent of frequency suggesting long-range ordering. The isothermal magnetization at 2 K increases gradually with field without saturation at 5 T and shows a small hysteresis of 340 Oe and remanant magnetization of 0.334 μ_B (Figure S21). The maximum magnetization value is 4.65 μ_B, which is close to that expected for two Co(II) ions of 4.6 μ_B. These characteristics suggest a ferromagnetic ground state,[34] which according to the discussion above consist of parallel octahedral Co1 moments. The low Curie temperature is consistent with the weaker exchange interaction between Co1 within the squares and even weaker Co1−Co1 between squares via the oxidized diamagnetic Co2.

Hence, the magnetism appears to be little affected by the different solvents as **1**·3DMF and **1**·*x*Solvent all show canted-antiferromagnetism, but their presence is important to provide weak antiferromagnetic interchain couplings to give a long-range ordered ground state (Figure 6). By removing the guests those weak couplings are turned off, and the magnetism is that of noninteracting chains, therefore a superparamagnetic state akin single-chain magnetism is observed. By modifying the geometry through coordination of H_2O to a more regular octahedron for Co1, the strength of the Co1−Co1 and Co1−Co2 is drastically reduced, and in addition anisotropy of Co1 is elevated. These structural and magnetic anisotropy changes result in a ferrimagnetic state due to a ferromagnetic interchain coupling. Upon partial oxidation of the tetrahedral Co2 site that results in it becoming diamagnetic (d^6, S = 0), a ferromagnetic state is stabilized, as the interchain coupling is ferromagnetic.

4. CONCLUSION

$[Co^{II}_3(pybz)_2(lac)_2]$ as its Zn analogue is one of the most stable MMOFs due to its very strong square rod of Co-lactate and the double wall connection between them. Single-crystal to single-crystal transformation confirms the removal of the solvents and the porous channels can house different solvents (DMF, methanol, ethanol, propanol and benzene) and gases (N_2, H_2 and CH_4) reversibly. Post-synthetic modification with water changes the geometry of the cobalt, while I_2 in DMSO/H_2O partially oxidized the metal ions. Raman spectroscopy confirms these structural changes. The magnetism resulted for the first time in the observation of four magnetic ground states in any material, canted antiferromagnets for $[Co^{II}_3(pybz)_2(lac)_2]$·*x*Solvent and iodine-loaded samples due to the interchain coupling (J') via the solvent or iodine molecules being negative, single-chain magnet for the desolvated $[Co^{II}_3(pybz)_2(lac)_2]$ as J' approached 0, ferrimagnet for $[Co^{II}_3(pybz)_2(lac)_2(H_2O)_2]$·$7H_2O$ as $J' > 0$, and ferromagnet for the partially oxidized $[Co^{III}Co^{II}_2(pybz)_2(lac)_2(H_2O)_2]I$·$2H_2O$·1.5DMSO as $J' > 0$. In addition, the iodine-loaded $[Co^{II}_3(pybz)_2(lac)_2]$·$2.7I_2$ is a weak conductor. This family of compounds derived from a single framework is unique in its stability, gas sorption, and solvent exchange and especially its stabilization of four magnetic ground states as well as introducing electrical conductivity in a MMOF. It also presents a vivid example of chemically driven dynamic magnetic MMOFs. We believe that the different chemistry bringing in multifunctionalities in MMOFs will be useful in the development of emergent materials for the future.

■ ASSOCIATED CONTENT

Supporting Information

Addition files: crystal data in CIF files, TG, PXRD, sorption data of H_2 and CH_4, magnetic properties of **1**·*x*Solvent and **1**·$2.7I_2$, isothermal magnetization and hysteresis loops of **1**·3DMF, **1**, **1a**·$7H_2O$, and **1b**·I^-·$2H_2O$·1.5DMSO. This material is available free of charge via the Internet at http://pubs.acs.org.

■ AUTHOR INFORMATION

Corresponding Author

zmh@mailbox.gxnu.edu.cn

Notes

The authors declare no competing financial interest.

■ ACKNOWLEDGMENTS

This work was supported by NSFC (nos. 21371037, 91122032), funds for doctoral discipline of university (20134504110001), Guangxi Province Science Funds for Distinguished Young Scientists (2012GXNSFFA060001), and the Project of Talents Highland of Guangxi Province as well as the Project of Talents Highland of Colleges and Universities in Guangxi Province. M.K. is supported by CNRS-France.

■ REFERENCES

(1) (a) Thematic issue of metal-organic frameworks.*Chem. Rev.* **2012**, *112*, 673−1268. (b) Metal-organic frameworks issue. *Chem. Soc. Rev.* **2009**, *38*, 1201−1508.

(2) (a) Meek, S. T.; Greathouse, J. A.; Allendorf, M. D. 2011, *23*, 249-267. (b) Cheetham, A. K.; Rao, C. N. R. *Science* **2007**, *318*, 58−59.

(3) (a) Coronado, E.; Dunbar, K. R. *Inorg. Chem.* **2009**, *48*, 3293−3896. (b) Yamada, T.; Otsubo, K.; Makiura, R.; Kitagawa, H. *Chem. Soc. Rev.* **2013**, *42*, 6655−6669. (c) Dechambenoit, P.; Long, J. R. *Chem. Soc. Rev.* **2011**, *40*, 3249−3265. (d) Leong, W. L.; Vittal, J. J. *Chem. Rev.* **2011**, *111*, 688−764. (e) Wang, Z. M.; Hu, K. L.; Gao, S.; Kobayashi, H. *Adv. Mater.* **2010**, *22*, 1526 and references cited therein. (f) Hang, T.; Zhang, W.; Ye, H. Y.; Xiong, R. G. *Chem. Soc. Rev.* **2011**, *40*, 3577−3598.

(4) (a) Goodenough, J. B. *Magnetism and the Chemical Bond*; John Wiley and Sons: New York, 1963. (b) Kahn, O. *Molecular Magnetism*; VCH Publishers, Inc.: New York, 1993. (c) Kaye, S. S.; Choi, H. J.; Long, J. R. *J. Am. Chem. Soc.* **2008**, *130*, 16921−16925. (d) Wang, X. Y.; Wang, Z. M.; Gao, S. *Chem. Commun.* **2008**, 281−294.

(5) Wang, Z.; Zhang, B.; Fujiwara, H.; Kobayashi, H.; Kurmoo, M. *Chem. Commun.* **2004**, 416−417.

(6) Kurmoo, M. *Chem. Soc. Rev.* **2009**, *38*, 1353−1379.

(7) Kurmoo, M.; Kumagai, H.; Chapman, K. W.; Kepert, C. J. *Chem. Commun.* **2005**, 3012−3014.

(8) Kurmoo, M.; Kumagai, H.; Akita-Tanaka, M.; Inoue, K.; Takagi, S. *Inorg. Chem.* **2006**, *45*, 1627−1637.

(9) (a) Halder, G. J.; Kepert, C. J.; Moubaraki, B.; Murray, K. S.; Cashion, J. D. *Science* **2002**, *298*, 1762−1765. (b) Cheng, X. N.; Zhang, W. X.; Lin, Y. Y.; Zheng, Y. Z.; Chen, X. M. *Adv. Mater.* **2007**, *19*, 1494−1498.

(10) (a) Sun, H. L.; Wang, Z. M.; Gao, S. *Coord. Chem. Rev.* **2010**, *254*, 1081−1100. (b) Bogani, L.; Vindigni, A.; Sessoli, R.; Gatteschi, D. *J. Mater. Chem.* **2008**, *18*, 4750−4758.

(11) (a) Gatteschi, D.; Sessoli, R. *Angew. Chem., Int. Ed.* **2003**, *42*, 268−297. (b) Clérac, R.; Miyasaka, H.; Yamashita, M.; Coulon, C. *J. Am. Chem. Soc.* **2002**, *124*, 12837−12844. (c) Zeng, M. H.; Yao, M. X.; Liang, H.; Zhang, W. X.; Chen, X. M. *Angew. Chem., Int. Ed.* **2007**, *46*, 1832−1835.

(12) (a) Wriedt, M.; Yakovenko, A. A.; Halder, G. J.; Prosvirin, A. V.; Dunbar, K. R.; Zhou, H. C. *J. Am. Chem. Soc.* **2013**, *135*, 4040−4050. (b) Mohapatra, S.; Rajeswaran, B.; Chakraborty, A.; Sundaresan, A.; Maji, T. K. *Chem. Mater.* **2013**, *25*, 1673−1679. (c) Ferrando-Soria, J.; Ruiz-García, R.; Cano, J.; Stiriba, S.-E.; Vallejo, J.; Castro, I.; Julve, M.;

Lloret, F.; Amorós, P.; Pasán, J.; Ruiz-Pérez, C.; Journaux, Y.; Pardo, E. *Chem.—Eur. J.* **2012**, *18*, 1608−1617.
(13) Ouellette, W.; Prosvirin, A. V.; Whitenack, K.; Dunbar, K. R.; Zubieta, J. *Angew. Chem., Int. Ed.* **2009**, *48*, 2140−2143.
(14) Zeng, M.-H.; Wang, Q.-X.; Tan, Y.-X.; Hu, S.; Zhao, H.-X.; Long, L.-S.; Kurmoo, M. *J. Am. Chem. Soc.* **2010**, *132*, 2561−2563.
(15) Cohen, S. M. *Chem. Rev.* **2012**, *112*, 970−1000 and references therein.
(16) Sun, F.; Yin, Z.; Wang, Q. Q.; Sun, D.; Zeng, M. H.; Kurmoo, M. *Angew. Chem., Int. Ed.* **2013**, *52*, 4538−4543.
(17) Macrae, C. F.; Bruno, I. J.; Chisholm, J. A.; Edgington, P. R.; McCabe, P.; Pidcock, E.; Rodriguez-Monge, L.; Taylor, R.; Streek, J.; Wood, P. A. *J. Appl. Crystallogr.* **2008**, *41*, 466−470.
(18) Sheldrick, G. M. *SADABS 2.05*; University of Göttingen: Göttingen, Germany; 2002.
(19) *SHELXTL 6.10*; Bruker Analytical Instrumentation: Madison, WI, 2000.
(20) *PLATON, A Multipurpose Crystallographic Tool*; Utrecht University: Utrecht, The Netherlands, 2001: Spek, A. L. *J. Appl. Crystallogr.* **2003**, *36*, 7−13.
(21) (a) Zeng, M. H.; Feng, X. L.; Zhang, W. X.; Chen, X. M. *Dalton Trans.* **2006**, 5294−5303. (b) Zeng, M. H.; Zhou, Y. L.; Wu, M. C.; Sun, H. L.; Du, M. *Inorg. Chem.* **2010**, *49*, 6436−6442.
(22) (a) Kurmoo, M. *Chem. Mater.* **1999**, *11*, 3370−3378. (b) Kurmoo, M. *J. Mater. Chem.* **1999**, *9*, 2595−2599. (c) Kurmoo, M. *Phil. Trans. A* **1999**, *357*, 3041−3061.
(23) Nakamoto, K. *Infrared and Raman Spectra of Inorganic and Coordination Compounds*; John Wiley and Sons: New York, 2009, pp 1−222.
(24) Zeng, M. H.; Tan, Y. X.; He, Y. P.; Yin, Z.; Chen, Q.; Kurmoo, M. *Inorg. Chem.* **2013**, *52*, 2353−2360.
(25) (a) Mehlana, G.; Ramon, G.; Bourne, S. A. *CrystEngComm* **2013**, *15*, 9521−9529. (b) Mehlana, G.; Bourne, S. A.; Ramon, G. *Dalton Trans.* **2012**, *41*, 4224−4231.
(26) (a) Ryu, D. W.; Lee, W. R.; Lee, J. W.; Yoon, J. H.; Kim, H. C.; Koh, E. K.; Hong, C. S. *Chem. Commun.* **2010**, *46*, 8779−8781. (b) Barthelet, K.; Marrot, J.; Riou, D.; Férey, G. *Angew. Chem., Int. Ed.* **2002**, *41*, 281−284.
(27) Horike, S.; Shimomura, S.; Kitagawa, S. *Nat. Chem.* **2009**, *1*, 695−704.
(28) Hertzsch, T.; Budde, F.; Weber, E.; Hulliger, J. *Angew. Chem., Int. Ed.* **2002**, *41*, 2281−2284.
(29) (a) Choi, H. J.; Suh, M. P. *J. Am. Chem. Soc.* **2004**, *126*, 15844−15851. (b) Ohtani, R.; Yoneda, K.; Furukawa, S.; Horike, N.; Kitagawa, S.; Gaspar, A. B.; Muñoz, M. C.; Real, J. A.; Ohba, M. *J. Am. Chem. Soc.* **2011**, *133*, 8600−8605. (c) Horike, S.; Sugimoto, M.; Kongpatpanich, K.; Hijikata, Y.; Inukai, M.; Umeyama, D.; Kitao, S.; Seto, M.; Kitagawa, S. *J. Mater. Chem. A* **2013**, *1*, 3675−3679.
(30) Zeng, M. H.; Zhang, W. X.; Sun, X. Z.; Chen, X. M. *Angew. Chem., Int. Ed.* **2005**, *44*, 3079−3082.
(31) (a) Feng, X. W.; Liu, J. J.; Harris, T. D.; Hill, S.; Long, J. R. *J. Am. Chem. Soc.* **2012**, *134*, 7521−7529. (b) Chen, Q.; Zeng, M. H.; Zhou, Y. L.; Zou, H. H.; Kurmoo, M. *Chem. Mater.* **2010**, *22*, 2114−2119.
(32) (a) Coulon, C.; Miyasaka, H.; Clérac, R. In *Structure and Bonding*; Winpenny, R., Ed.; Springer-Verlag: Berlin, 2006, 163−206. (b) Miyasaka, H.; Clérac, R. *Bull. Chem. Soc. Jpn.* **2005**, *78*, 1725−1748. (c) Miyasaka, H.; Julve, M.; Yamashita, M.; Clérac, R. *Inorg. Chem.* **2009**, *48*, 3420−3437. (d) Miyasaka, H.; Yamashita, M. *Dalton Trans.* **2007**, 399−406. (e) Zhang, W. X.; Ishikawa, R.; Breedlove, B.; Yamashita, M. *RSC Adv.* **2012**, 1−27. (f) Bogani, L.; Vindigni, A.; Sessoli, R. *J. Mater. Chem.* **2008**, *18*, 4750−4758.
(33) (a) Zeng, M. H.; Wu, M. C.; Liang, H.; Zhou, Y. L.; Chen, X. M.; Ng, S. W. *Inorg. Chem.* **2007**, *46*, 7241−7243. (b) Zhang, B.; Wang, Z. M.; Kurmoo, M.; Gao, S.; Inoue, K.; Kobayashi, H. *Adv. Funct. Mater.* **2007**, *17*, 577−584.
(34) Weng, D. F.; Wang, Z. M.; Gao, S. *Chem. Soc. Rev.* **2011**, *40*, 3157−3181.